

Comparison of Tropical Pacific Temperature And Current Simulations With Two Vertical Mixing Schemes Embedded In An Ocean General Circulation Model And Reference To Observations

David Halpern¹, Yi Chao^{2,3}, Chung-Chun Ma² and Carlos R. Mechoso²

¹ Earth and Space Sciences Division

Jet Propulsion Laboratory

California Institute of Technology

Pasadena, CA 91109

² Department of Atmospheric Sciences

University of California

Los Angeles, CA 90024

³ Now at Earth and Space Sciences Division

Jet Propulsion Laboratory

California Institute of Technology

Pasadena, CA 91109

Abstract. The Pacanowski-Philander (PP) and Mellor-Yamada (MY) parameterization models of vertical mixing by turbulent processes were embedded in the Geophysical Fluid Dynamics Laboratory high-resolution ocean general circulation model of the tropical Pacific Ocean. All other facets of the numerical simulations were the same. Simulations were made for the 1987 - 1988 period. At the equator, the MY simulation produced near surface temperatures more uniform with depth, a deeper thermocline, a deeper core speed of the Equatorial Undercurrent, and a South Equatorial Current with greater vertical thickness compared to that computed with the PP method. Along 140°W between 5°N and 10°N, both simulations were the same.

Moored-buoy current and temperature observations had been recorded by the Pacific Marine Environmental Laboratory at three sites (165°E, 140°W, 100°W) along the equator and at three sites (5°N, 7°N, 9°N) along 140°W. Simulated temperatures were lower than those observed in the near surface layer, and higher than those observed in the thermocline. Temperature simulations were in better agreement with observations compared to current simulations. At the equator, PP current and temperature simulations were more representative of the observations than MY simulations.

1. Introduction

A key component for the success of ocean general circulation model (OGCM) simulations of upper ocean current and temperature fields is the representation or parameterization, in terms of large-scale variables, the turbulent motions and other physical processes occurring at scales smaller than the model grid. Vertical mixing of heat, salt and momentum by turbulent processes is a very important phenomenon to parameterize, and many parameterization schemes exist. Some are based on turbulent kinetic energy [Mellor and Yamada, 1982; Gaspar et al., 1990], Richardson number [Pacanowski and Philander, 1981], Richardson number and wind friction velocity [Reason et al., 1993], one-dimensional mixed layer dynamics [Kraus and Turner, 1967], observations of mixing [Peters et al., 1988], and combinations of the methods [Stockdale et al., 1993]. The Pacanowski and Philander [1981] method, hereafter named "PP", and Mellor and Yamada [1982] scheme,

hereafter named "MY", are widely used in uncoupled OGCM [Stockdale *et al.*, 1993] and coupled ocean-atmosphere GCM [Neelin *et al.*, 1992] simulations. A low MY and PP simulations of temperature and zonal current fields in the tropical Pacific compare with each other, and with observations, is addressed in this paper. The study encompassed the 1987-1988 interval containing El Niño and La Niña. Moored-buoy current and temperature data were recorded by the Pacific Marine Environmental Laboratory along the equator at 165°W, 140°W and 110°W [McPhaden and Hayes, 1990; McPhaden *et al.*, 1990] and along 140°W at 5°N, 7°N, and 9°N.

The two OGCM simulations differ only in the formulation of the parameterization of vertical mixing by turbulent processes. In the PP parameterization the vertical diffusivity and viscosity are functions of the local Richardson number because of a belief that vertical mixing is strongly influenced by vertical shear of the mean currents. In the upper 100 m of the model, the coefficient of vertical eddy viscosity has a minimum value to compensate for mixing by the high-frequency wind fluctuations which are absent from the monthly mean winds. The PP parameterization is an ad hoc simple solution to include turbulent mixing, in a GCM. The PP scheme employed in our analysis had the same coefficients used by Philander *et al.* [1987]. In contrast to the simplified representation of mixing portrayed by the PP scheme, turbulence closure models attempt to explicitly model the turbulent transports of heat, salt and momentum in terms of the larger scale fields. The MY parameterization code developed by Rosati and Miyakoda [1988] was used.

The Philander-modified version of the Bryan [1969] - Semtner [1974] - Cox [1984] OGCM [Philander *et al.*, 1987] covers the Pacific Ocean from 30°S to 5°N with realistic coastal geometry. The model ocean has a constant depth of 4149 m. A rigid lid approximation is made at the surface. The longitudinal resolution is 10°. The latitudinal grid size is 1/3° within 10°S and 10°N, and gradually increases poleward to 2.5° at 30°S and 50°N. Coefficients of horizontal eddy viscosity and eddy diffusivity between 10°S and 10°N are $2 \times 10^3 \text{ m}^2 \text{ s}^{-1}$. There are 27 levels throughout the water column with 10 uniform layers in the upper 100 m and 8 additional levels between 100 and 317 m. The model time step is 1 hour, and 3-day average temperature, salinity, and horizontal

velocity components are stored. A model year has 365 days, or 120 intervals of 3.04 days. A model month was equal to ten consecutive 3.04-day intervals.

Initial conditions of the OGCM temperature and salinity distributions were the *Levitus* [1982] climatological-mean January distributions. The model ocean was initially at rest. For the first three years of simulation the model ocean was forced with the *Hellerman and Rosenstein* [1983] climatological-mean monthly surface wind stress and the *Oort et al.* [1987] climatological-mean monthly surface air temperature. Surface heat flux was computed according to the method described by *Philander et al.* [1987]. No surface salt flux was imposed on the OGCM. Simulated oceanic conditions at the end of the third year became the initial conditions for the 1986-1988 simulations. Simulations for 1986 were used elsewhere and we have not explored the effect of beginning the simulations in January 1986 instead of a year later. For the 1986-1988 simulations, the model ocean was forced with surface air temperature from the European Centre for Medium-Range Weather Forecasting and surface wind stress computed from the Florida State University (FSU) monthly mean $2.0^\circ \times 2.0^\circ$ pseudostress component fields [Goldenberg and O'Brien, 1981] by using a constant drag coefficient (1.4×10^{-3}). This value is about 15% higher than the value suggested by *Trenberth et al.* [1989]. In computing the wind stress the speed of the water is assumed negligible compared with the wind speed, which creates an uncertainty of the monthly wind stress along the equator as large as 17% for several months [Halpern, 1988].

2. Results

2.1. Temperature Along Equator

Figure 1 displays the annual mean MY and PP temperature differences at the equator corresponding to 1988, because these differences were larger than in 1987. Differences between PP and MY sea surface temperatures (SS'1'), i. e., the 0-10 m average temperature, were negligible. Temperature differences greater than 1°C occurred from 25-100 m and from 150°W to 85°W because depths of MY $15\text{-}20^\circ\text{C}$ isotherms were 10-20 m deeper than PP isotherms.

Maximum temperature differences (3-4°C) were confined to a thin (10 m) interval near 35 m depth and a narrow longitudinal band (15° wide) in the eastern Pacific near 95°W.

At 110°W in 1987 (Figure 2a), MY temperatures at 10, 25 and 35 m were 0.6°C more representative of the moored-buoy observations, named "MB", than 1'1' temperatures. Also, MY and MB near surface temperatures displayed near-zero vertical gradients. In 1988 at 110°W (Figure 2b), MY temperatures at 10 and 25 m again indicated a near-zero vertical gradient; however, 1'1' and MB temperatures indicated that the thermocline reached the surface.

Simulated temperatures above 50 m were less than that observed, named "cold bias", and simulated temperatures below 75 m were higher than observations, named "warm bias" (Figure 2). Maximum cold and warm biases were 2.2°C (45 m, 110°W, 1987) and 2.7°C (12.0 m, 140°W, 1988), respectively. Biases caused the simulated temperature gradient between the surface and 150 m to be weaker than that observed at 140°W and 110°W.

There were 581 monthly mean MB values at 165°E, 140°W and 110°W. The MB and MY bias (0.8°C) was significant, according to Student's t-test [Press *et al.*, 1986]. The 95% significance level is used throughout the paper. The MB and PP bias (0.4°C) was not significant, indicating a better correspondence between MB and PP temperatures. Correlation coefficients between MB and PP and between MB and MY were equal and high (0.94). Root-mean-square (rms) differences between MB and PP and between MB and MY were equal and large (1.9°C).

The amplitude of the annual period fluctuation of the 10-m temperature, T_{10m} , during 1987-1988 was determined by harmonic analysis in which we assume the existence of an annual period fluctuation of the form $(T_{10m})_a \sin(\omega t - \phi)$, where $(T_{10m})_a$ is the amplitude, ω is the annual angular frequency ($= 3600/12$), t is the time, in months, and ϕ is the phase lag in degrees. At 110°W the MB, MY and 1'1' amplitudes were about the same (1.6-1.8°C); at 140°W the amplitudes were approximately the same (1.0-1.1°C), but 40% smaller than at 110°W. The 10-m simulated annual cycle of temperature was not sensitive, to the MY or 1'1' parameterizations. Other vertical mixing schemes influence the annual fluctuation of SST in the tropical Pacific [(km *et al.*, 1994).

2.2. Temperature Along 140°W

in the 5°N - 10°N band where the North Equatorial Countercurrent (NECC) occurs, the MY 25, 26 and 27°C isotherms were more uniform with depth than the corresponding 1°1' isotherms, and the MY isotherms extended to greater depths compared to the PP isotherms (Figures 3a and 3b). Throughout the NECC the PP and MY differences were less than 1 °C (Figure 3c).

At 5°N (Figure 3d), the simulated temperatures at the depth (2.0 m) of the uppermost observation were 0.5-1.0°C lower than the observed temperature. Whether this situation represents a northward extension of the equatorial cold bias is unknown. In the center of the NECC at 7°N (Figure 3e), no cold bias occurred near the surface; however, at 9°N (Figure 3f), simulated temperatures at 20 and 45 m displayed a cold bias. The warm bias in the thermocline was largest (2°C) at 9°N and smallest at 7°N.

Most of the difference between simulated and observed temperatures within the thermocline at 5°N and 9°N were caused by a 3- to 4-month disturbance (not shown) that was not apparent in either simulation. At 7°N, the simulated and observed mean temperatures were fortuitously equal (Figure 3e) because the disturbance also appeared there. At 5°N, 7°N and 9°N, the departure between a monthly mean observed temperature and the nearly identical simulated temperatures reached 5°C. The correlation coefficient and rms difference between simulated and observed temperatures were 0.94 and 2.2°C, respectively, indicating the inability of either simulation to adequately reproduce the magnitude of the fluctuation. The origin of the disturbance, which could have been a north-south meandering of the NECC [Wyrtki, 1978], is unknown.

2.3. Current Along Equator

10 depths of the PP and MY Equatorial Undercurrent (EUC) core speed decreased from west to east along the equator across the entire width of the Pacific (Figures 4a and 4b). The 1°1' east-west slope of the depth of the core speed was larger and the 1°1' depth of the core speed was less than that simulated by MY, resulting in stronger vertical shear from the surface to the EUC core for PP compared to MY. The PP eastward current component was greater than MY above the depth of the

1 μ C core speed, except at about 5 m near 105°W (Figure 4c). Below the depth of the core speed, the 1°1' and MY shears were approximately equal.

The PP and MY annual mean differences in the zonal current component were larger in J 988 than in 1987, and the maximum difference (0.5-0.6 m s⁻¹), which was greater than one-half the 1 μ C core speed, occurred at about 65 m in the 145°W- J 30°W longitudinal band (Figure 4c). In 1987 the maximum difference (0.3-0.4 m s⁻¹) was also at about 65 m, but the position shifted eastward to 120°W- J 05°W.

We investigated whether the large point-to-point differences between PP and MY zonal currents (Figure 4c) appeared in integral properties of the 1 μ C and South Equatorial Current (SEC) at J 65°E, J 40°W and 110°W. The 2-year mean 1°1' 1 μ C transports per unit width were larger compared to MY by about 6% (13 m² s⁻¹). The opposite situation was found for the SEC because the MY transport per unit width was greater than 1°1' by about 27% (4 m² s⁻¹). The 1°1' and MY vertical thicknesses of the 1 μ C were almost the same (235 m), in marked contrast to the 50% difference between the PP and MY vertical thicknesses of the SEC. The PP 1 μ C transport (32 x 10⁶ m³ s⁻¹, or 32 Sv) was nearly 4 Sv, or about 13%, greater than the MY value, and the difference (5.8 Sv) was not much greater than the bias. The correlation coefficient between 1°1' and MY 1 μ C total transports was 0.95.

At J J 0°W during both years the 1°1' annual mean zonal current profiles were more representative of the observations with regard to current speed and shear compared to the MY simulation (Figure 5). At 140°W, the 1°1' and MY currents were similar, except at 80 m where the MY eastward current was too small by 0.3 m s⁻¹ in J 987 and 0.5 m s⁻¹ in 1988 compared to the observations. At 165°E, the PP and MY differences were negligible in J 987, and in 1988 the MY currents at 50 and 100 m were more representative of the observations.

On many occasions the monthly mean observed and simulated zonal currents differed by more than 0.5 m s⁻¹ (not shown). At 110°W, the 10-m simulated annual mean westward current was 2-3 times greater than that observed (Figure 5) because the simulations did not adequately reveal the observed eastward flow in March-May that is associated with the annual Kelvin wave.

There were 341 monthly mean MB values at 165°E , 140°W and 110°W . The MB and 1'1' zonal current bias (0.02 m s^{-1}) was not significant, and the MB and MY bias (0.13 m s^{-1}) was significant. The 1'1' monthly mean zonal current at 165°E , 140°W and 110°W was more representative of the observations compared to MY,

2.4. Current Along 140°W

The 1988 mean PP and MY zonal current components throughout the NJ ICC had differences that were less than 0.05 m s^{-1} (not shown). At 7°N near the middle of the NJ ICC, simulated currents at 20 and 40 m were 0.15 m s^{-1} larger than observations (Figure 6), and this feature was persistent each month. The observed current was almost uniform between 20 and 80 m, in contrast to the large simulated shear ($2 \times 10^{-3} \text{ s}^{-1}$). Differences between simulated and observed current decreased with depth and were nonexistent at the 20(-111 bottom of the NJ ICC).

3. Discussion

3.1. Simulations

Vertical profiles of upper ocean zonal current and temperature at the equator are sensitive to the vertical mixing of momentum and heat. For example, the EUC thickness is too small and the maximum speed is too large if the vertical turbulent momentum flux is too small [McCreary, 1981]. The situation is expected to be different in the NJ ICC which is in geostrophic balance, although important nongeostrophic components exist [Johnson *et al.*, 1988].

That the MY model created increased mixing compared to the PP technique was illustrated by the smaller shear above the depth of the EUC core speed (Figures 4a and 4b), deeper penetration of the westward-flowing SIC (Figures 4a and 4b), and a more vertically homogeneous temperature profile. (Figures 2 (110°W), 3a, and 3b). Differences between 1'1' and MY zonal currents were much larger within the EUC and SIC compared to the NJ ICC (Figures 5 and 6). The PP and MY current bias was significant at the equator but not at 7°N , and the rms difference between 1'1' and

MY currents was significantly larger at the equatorial sites compared to 7°N. Point-to-point differences between PP and MY EUC simulations were substantial (Figure 4c); however, integral characteristics of the EUC, such as vertical thickness and total transport, agreed within 15%.

3.2. Observations and Simulations

3.2.1. Longitudinal Variations. That the 1°1' zonal current and temperature along the equator were more representative of observations compared to MY was not a surprise because the PP scheme had been tuned for the equatorial Pacific [*Pacanowski and Philander, 1981*]. The 1°1' scheme favors regions where the current has large vertical shear. The 1987 mean maximum MB vertical shears, which were computed in the interval defined by current-meter depths, were 0.5, 1.3 and $1.3 \times 10^{-2} \text{ s}^{-1}$ at 165°E, 140°W and 110°W, respectively. At 165°E, where the maximum vertical shear was nearly 60% smaller than at 140°W and 110°W, the 1°1' and MY zonal currents were approximately equal, in contrast to the situation at 140°W and 110°W where PP currents were more representative of MB (Figure 5). Also, at 7°N, 140°W where the maximum MB shear ($0.2 \times 10^{-2} \text{ s}^{-1}$) was less than that at 165°E, the PP and MY zonal currents were the same (Figure 6).

Comparison of observed and simulated near surface temperatures is sensitive to the longitude along the equator of the intercomparison test. The rms differences between 10-m observed and simulated temperatures in 1987 and 1988 were 1.5 and 2.4°C at 140°W and 110°W, respectively; the difference was significant. In addition, the correlation coefficient between observed and simulated 10-m temperatures was significantly higher at 140°W than at 110°W.

3.2.2. Cold Bias. In the approximate 50-m near surface layer on the equator at 140°W and 110°W, the simulated temperatures were lower than that observed during the 1987 El Niño but not during the 1988 La Niña (Figure 2). Why the cold bias had a year-to-year variation is beyond the scope of this report.

Possible causes of the cold bias are excessive upward advection of cold water, too-low heat flux into the ocean, excessive westward advection of cold water, and incorrect OGCM physics of the upper ocean heat budget. To reconcile some features of the temperature profile, the vertical

velocity was computed from the simulated east-west and north-south components of velocity using the equation of continuity with zero vertical motion at the surface. The simulated maximum upwelling velocities at 140°W and 11°W (Figure 7) were about 1.5 times greater than that observed several years earlier [Halpern and Freitag, 1987; Halpern et al., 1989], which are referenced because vertical velocity was not measured during 1987 and 1988. Uplifting the simulated thermocline by a greater amount would lead to near surface temperatures that would be lower than observed, although we can not separate the relative contributions produced by upwelling and mixing of the uplifted thermocline.

Another factor that likely influenced the simulation of temperature, especially at 10 m, is the neglect of the surface zonal current in calculating surface zonal wind stress, which is applied as a body force to the uppermost 10-m layer of the OGCM. The 17% variation in surface wind stress that is associated with the surface current [Halpern, 1988] is approximately the same as the uncertainty of the drag coefficient, and is sufficient to alter an OGCM simulation of SST by about 2°C [Harrison et al., 1990]. The 1987-1988 average MY cold bias at 10 m at 11°W was 17% larger in March-May than in September-November, which is consistent with the idea that the sulfate zonal current was not included in the computation of the surface wind stress.

We investigated whether salinity could be a factor contributing to the cold bias. Vertical profiles of PP and MY annual mean salinities from the surface to 300 m for 1987 and 1988 at 11°W were similar. Salinity measurements [Hayes et al., 1991] indicated stronger near surface salinity gradient and less saline near surface water compared to simulations. This inhibits vertical mixing and contributes towards elevated near surface temperatures compared to those simulated.

3.2.3. Warm Bias. Within the equatorial thermocline at 165°E , 140°W and 11°W , simulated temperatures were higher than observed (Figure 2). One reason for the warm bias is that observed upwelling speeds at 150 m at 140°W [Halpern et al., 1989] and 11°W [Halpern and Freitag, 1987], which were not made during 1987-1988, were greater than simulated values (Figure 7). Thus, the simulated thermocline would be deeper than observed. Another possible contribution to the warm bias is mixing created by the breaking of short-period internal gravity

waves [Moum *et al.*, 1992]. The OGCM employed in this analysis did not contain a parameterization of short-period internal waves.

3.3. Comparison With Other Studies

We are aware of results from one similar kind of investigation. The $1^{\circ}1'$ and MY zonal current differences displayed in Figure 4c are different than those computed by *Delecluse et al.* (Figure 3.3.2.c in *Stockdale et al.* [1993]) from OGCM simulations with the *Gaspar et al.* [1990] turbulent kinetic energy, named "TKE", and $1^{\circ}1'$ parameterizations for vertical mixing. In their result, the isoline of zero difference between $1^{\circ}1'$ and TKE zonal currents was approximately linear from 300 m near $150^{\circ}E$ to 25 m near $120^{\circ}W$. This yielded a 0.7 m s^{-1} difference at 60 m near $90^{\circ}W$, in contrast to the near zero difference between PP and MY currents at 60 m near $90^{\circ}W$ (Figure 4c). In their result (Figures 3.3.2.a and 3.3.2.b in *Stockdale et al.* [1993]), the TKE EUC core speed was 20% greater than the PP value, in contrast to our investigation in which the MY EUC core speed was 10% less than the $1^{\circ}1'$ value (Figures 4a and 4b). The apparent disagreement between our results and those of *Delecluse et al.* could be influenced by experimental design. Our OGCM had six additional layers above 160 m. Also, different levels of complexity of turbulent kinetic energy models were employed. The MY 2.5-level scheme contains three-dimensional diffusion and advection, and the 1.5-level TKE model does not include the effects of horizontal shear and horizontal turbulent diffusion. *Smith and Hess* [1993] have shown that a change of the *Mellor and Yamada* [1982] model from level 2, in which advection and diffusion of turbulent kinetic energy are ignored, to level 2.5 significantly alters the mixing regime. Differences between our analyses and those by *Delecluse et al.* need further investigation.

4* conclusion

At the equator, $1^{\circ}1'$ and MY simulated current and temperature had three generic differences: (i) MY mixing in the near surface layer was stronger, (ii) MY EUC core speed was deeper, and

(iii) MY SEC had a larger vertical thickness. No substantial difference was found between PP and MY simulations of integral properties of the current and temperature. Between 5°N and 9°N , PP and MY simulations of temperature and current were very similar.

Three generic features distinguish our simulations and observations: (i) warm bias occurred in the thermocline and a cold bias occurred in the near surface layer, (ii) temperature was better simulated than current, and (iii) agreement between PP and MB currents and temperatures at the equator was slightly better than that between MY and MB.

Temperature was not as good a discriminator as current because simulated and observed temperatures were more highly correlated compared to currents. The correlation coefficients between simulated and observed currents and temperatures at the three equatorial sites were 0.65 and 0.94, respectively, and the difference was significant. Also, in the NECC the correlation coefficients between simulated and observed currents and temperatures were 0.81 and 0.94, respectively, which were significantly different.

The PP and MY schemes have a number of adjustable parameters, and the simulation sensitivity to a range of values should be tested. That MY temperatures were more uniform with depth in the near surface layer compared to those of PP indicates the PP minimum level of mixing was too small; a similar conclusion was reached by *Richardson and Philander [1987]*.

In addition to further attention devoted to vertical mixing, parameterization, increased accuracy of simulated current and temperature require high frequency and high wavenumber components of the surface wind field, parameterization of internal gravity wave motion, and representation of salinity flux. Studies of the sensitivity of the EUC to the parameterization of horizontal mixing by turbulent processes are warranted because the maximum speed of the EUC is 25% greater for a doubling of the horizontal eddy viscosity coefficient [*Pacanowski and Philander, 1981*]. However, it is a tenet of faith that assimilation of observations will mitigate imperfect surface wind stress and OGCM physics and will yield improved simulations of subsurface temperature and current.

Acknowledgements. We are grateful to *III.* G. Philander, Princeton University, and W. Iurlin, GFDL, for extensive support and help during the OGCM transfer from a CYBER to a CRAY. Dr. A. Rosati, GFDL, kindly provided the computer code of the MY parameterization. Dr. M. McPhaden, PMEL, kindly sent the moored current and temperature data. W. Knauss, JPL, prepared diagrams in his usual outstanding fashion. We thank Dr. Philander, Dr. Rosati, and I. X. N. Smith, Australian Bureau of Meteorology Research Center, and two anonymous reviewers for helpful comments. This work was supported by DOE (Grant DE-FG03-91ER61214 (CCM, CRM)), NASA (UPN 578-2.2-26 (DII); UPN 578-2.1-13 (1)11); JPL, Contract 958658 to UCLA (CRM, YC)), and ONR (Grant N00014-89-J-1845 (CCM, CRM)). The research described in this paper was performed, in part, by the Jet Propulsion Laboratory, California Institute of Technology, under contract with the National Aeronautics and Space Administration.

References

- Bryan, K., A numerical method for the study of the world ocean, *Journal of Computational Physics*, 4, 347-376, 1969.
- Chen, D., A. J. Busalacchi, and L. Rothstein, The roles of vertical mixing, solar radiation, and wind stress in a model simulation of the sea surface temperature seasonal cycle in the tropical Pacific seasonal cycle, *Journal of Geophysical Research*, in press, 1994.
- Cox, M.D., A primitive, 3-dimensional model of the ocean, GFDL Ocean Group Technical Report No. 1, Geophysical Fluid Dynamics Laboratory, Princeton University, 143 pp., 1984.
- Gaspar, P., Y. Grégoris, and J.M. Lefevre, A simple eddy-kinetic-energy model for simulations of the ocean vertical mixing: Tests at station Papa and Long-Term Upper Ocean Study site, *Journal of Geophysical Research*, 95, 16179-16193, 1990.
- Goldenberg, S.B., and J.J. O'Brien, Time and space variability of tropical Pacific wind stress, *Monthly Weather Review*, 109, 1208-1218, 1981,

- Halpern, D., Moored surface wind observations at four sites along the Pacific equator between 140°W and 95°W, *Journal of Climate*, 1, 1251-1260, 1988.
- Halpern, D., and Halpern, P. Freitag, Vertical motion in the upper ocean of the equatorial eastern Pacific, *Oceanologica Acta*, 51%, 19-26, 1987.
- Halpern, D., R.A. Knox, D.S. Luther, and S.G.H. Philander, Estimates of equatorial upwelling between 140° and 110°W during 1984, *Journal of Geophysical Research*, 94, 8018-8020, 1989.
- Harrison, D.E., B. Geise, and E.S. Sarachik, Mechanisms of sea surface temperature change in the 1982-83 El Niño: Results from ocean general circulation model hindcasts, *Journal of Climate*, 3, 173-188, 1990.
- Hayes, S.P., L.J. Mangum, and K.E. Taggart, Repeat CTD measurements along PR16 - Part I, WOCE Notes, vol. 3, no. 4 (August), 1991. (Available from Department of Oceanography, Texas A&M University, College Station, Texas)
- Hellerman, S., and M. Rosenstein, Normal monthly wind stress over the world ocean with error estimates, *Journal of Physical Oceanography*, 13, 1093-1104, 1983.
- Johnson, E.S., L.A. Regier, and R.A. Knox, A study of geostrophy in tropical Pacific. Ocean currents during the NORPAX Tahiti Shuttle using a shipboard acoustic current doppler, *Journal of Physical Oceanography*, 18, 708-723, 1988.
- Kraus, E.B., and J.S. Turner, A one-dimensional model of the seasonal thermocline, *Tellus*, 19, 88-97, 1967.
- Levitus, S., Climatological atlas of the world ocean, NOAA Professional Paper No. 13, U. S. Government Printing Office, Washington, 173 pp., 17 fiche, 1982.
- Mellor, G.L. . . and T. Yamada, Development of a turbulence closure model for geophysical fluid problems, *Reviews of Geophysics and Space Physics*, 20, 851-875, 1982.
- McCreary, J., A linear stratified ocean model of the equatorial undercurrent, *Philosophical Transactions of the Royal Society of London*, 298, 603-635, 1981.

- McPhaden, M., and S. Hayes, Variability in the eastern equatorial Pacific Ocean during 1986-88, *Journal of Geophysical Research*, **95**, 13195-13208, 1990.
- McPhaden, M., S. Hayes, and L. Mangum, Variability in the western equatorial Pacific Ocean during the 1986-87 Niño/Southern Oscillation event, *Journal of Physical Oceanography*, **20**, 190-208, 1990.
- Moum, J.N., D. Hebert, C.A. Paulson, and D.R. Caldwell, Turbulence and internal waves at the equator. Part 1: Statistics from towed thermistors and a microstructure profiler, *Journal of Physical Oceanography*, **22**, 1330-1356, 1992.
- Neelin, J.D., M. Latif, *et al.*, Tropical air-sea interaction in general circulation models, *Climate Dynamics*, **7**, 73-104, 1992.
- Oort, R.A., Y. Pan, R.W. Reynolds, and C.F. Roplewski, Historical trends in the surface temperature over the oceans based on CCM2, *Climate Dynamics*, **2**, 29-38, 1987.
- Pacanowski, R., and S. G. Philander, Parameterization of vertical mixing in numerical models of tropical oceans, *Journal of Physical Oceanography*, **11**, 1443-1451, 1981.
- Peters, H., M.C. Gregg, and J.M. Toole, On the parameterization of equatorial turbulence, *Journal of Geophysical Research*, **93**, 1199-1218, 1988.
- Philander, S. G., W. Hurlin, and A.D. Seigel, A model of the seasonal thermocline in the tropical Pacific Ocean, *Journal of Physical Oceanography*, **17**, 1986-2002, 1987.
- Press, W.H., B.P. Flannery, S. A. Teukolsky, and W. T. Vetterling, *Numerical Recipes: The Art of Scientific Computing*, Cambridge University Press, 818 pp, 1986.
- Reason, C.J.C., I. Kuhnle, and B. Henderson-Sellers, A comparison of vertical mixing schemes embedded in an OGCM with application to air-sea interactions and the evolution of SST anomalies, *Meteorology and Atmospheric Physics*, **51**, 55-71, 1993.
- Richardson, P.L. and S.G. Philander, The seasonal variations of surface currents in the tropical Atlantic Ocean: A comparison of ship drift data with results from a general circulation model, *Journal of Geophysical Research*, **92**, 715-724, 1987.

- Rosati, A., and K. Miyakoda, A general circulation model for upper ocean simulation, *Journal of Physical Oceanography*, **18**, 1601-1626, 1988.
- Semtner, A. J., An oceanic general circulation model with bottom topography, Technical Report No. 9, Department of Meteorology, University of California, Los Angeles, 99 pp., 1974.
- Smith, N.R., and G.D. Mellor, A comparison of vertical eddy mixing parameterizations for equatorial ocean models, *Journal of Physical Oceanography*, **23**, 1823-1830, 1993.
- Stockdale, T., D. Anderson, M. Davey, P. Delecluse, A. Kattenberg, Y. Kitamura, M. Latif, and T. Yamagata, Intercomparison of tropical ocean GCMs, WCRP-79, WMO/TD-No. 545, World Meteorological Organization, Geneva, 43 pp + 53 figs., 1993.
- Trenberth, K.E., W.G. Large, and J.G. Olson, The effective drag coefficient for evaluating wind stress over the oceans, *Journal of Climate*, **2**, 1507-1516, 1989.
- Wyrtki, K., Lateral oscillations of the Pacific Equatorial Countercurrent, *Journal of Physical Oceanography*, **3**, 530-532, 1973,

Figure 1. Annual mean PP and MY temperature difference along the equator during 1988. Contour interval is 0.5°C , and negative values (dashed line) mean that the PP temperature was smaller than that of MY. Arrows show locations of moored-bmo observations along the equator.

Figure 2. Vertical distributions of annual mean $1^{\circ}\text{1}'$ and MY simulated and MB observed temperatures along the equator at 165°E , 140°W and 110°W for two (a) 1987 and (b) 1988.

Figure 3. Simulations of annual mean temperature along 140°W during 1988: (a) PP and (b) MY. (c) PP and MY temperature difference computed from (a) and (b), and negative values mean that the $1^{\circ}\text{1}'$ temperature was smaller than MY. Contour interval of (a), (b) and (c) is 1°C . (d) to (f) Vertical distributions of June-December 1988 $1^{\circ}\text{1}'$ and MY simulated and MB observed temperatures along 140°W at (d) 5°N , (e) 7°N , and (f) 9°N .

Figure 4. Simulations of annual mean zonal current (eastward is positive, solid line; westward is negative, dashed line) along the equator during 1988: (a) $1^{\circ}\text{1}'$ and (b) MY. (c) PP and MY difference computed from (a) and (b), anti positive values (solid lines) mean that the PP current was greater than that of MY. Contour interval of (a), (b) and (c) is 10 cm s^{-1} .

Figure 5. Vertical distributions of annual mean PP and MY simulated and MB observed zonal current component along the equator at 165°E , 140°W and 110°W for (a) 1987 and (b) 1988. Positive values are eastward and negative values are westward.

Figure 6. Vertical distributions of June-December 1988 $1^{\circ}\text{1}'$ and MY simulated and MB observed current at 7°N , 140°W . Positive values are eastward and negative values are westward.

Figure 7. Vertical distributions of 1987-1988 mean $1^{\circ}\text{1}'$ and MY vertical velocities along the equator at 165°E , 140°W and 110°W . Positive values are upward.

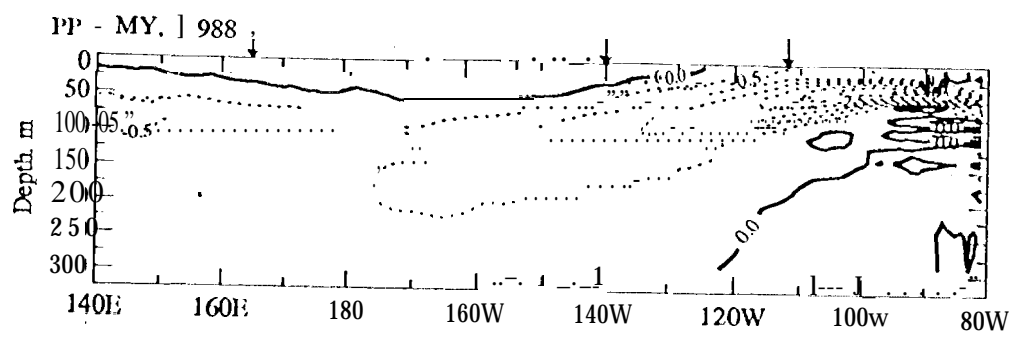
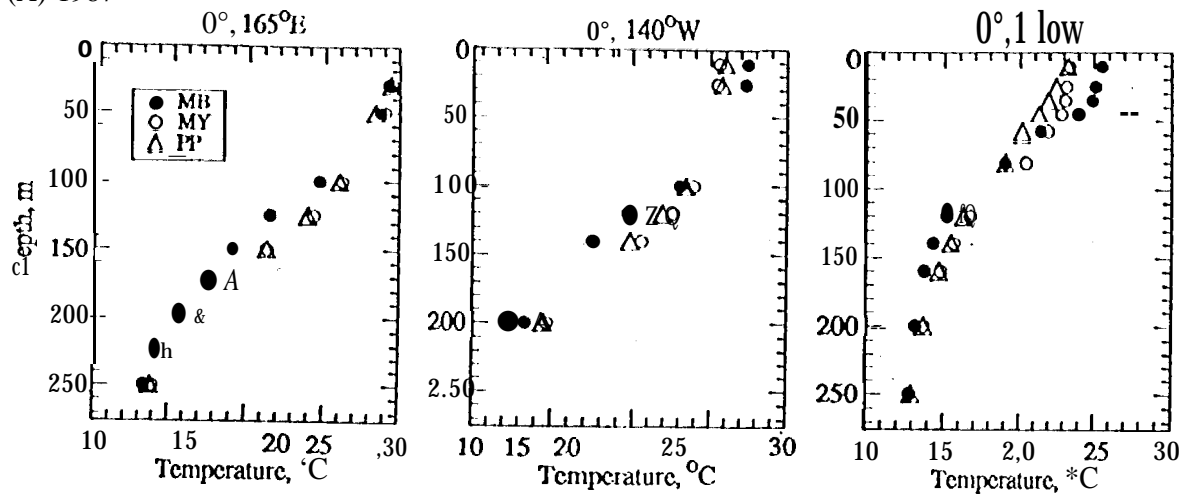


Figure 1

(A) 1987



(B) 1988

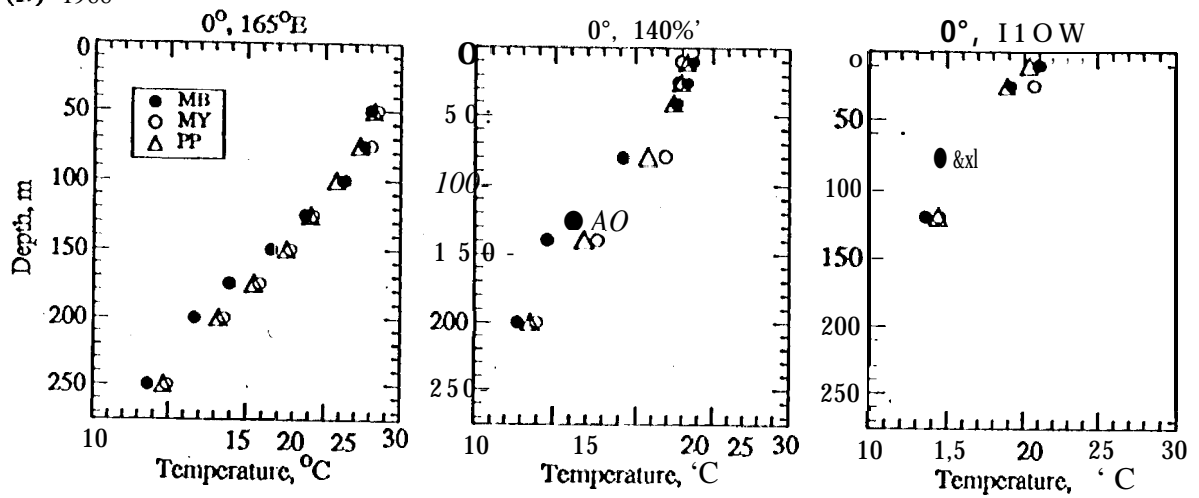


Figure 2

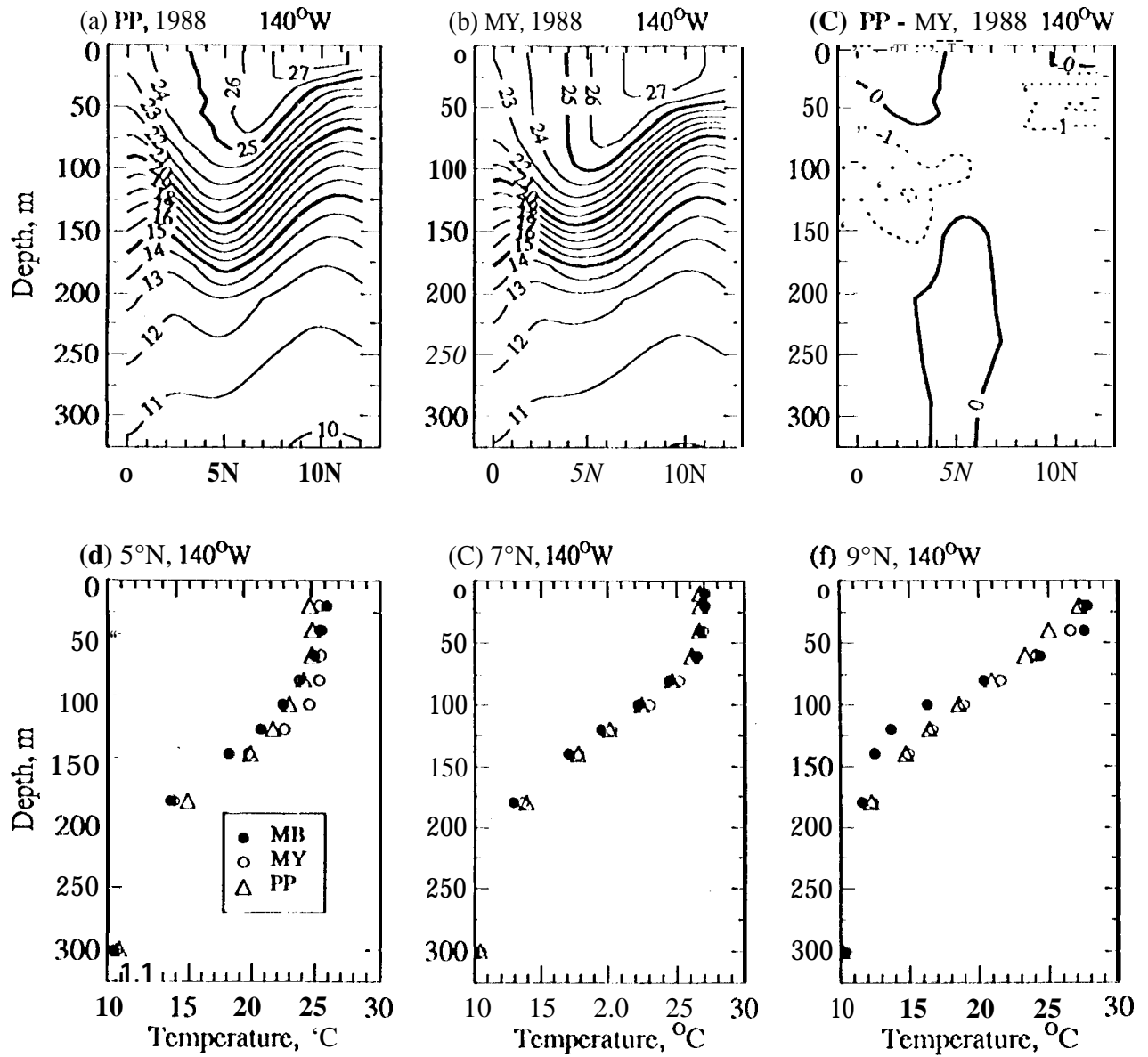
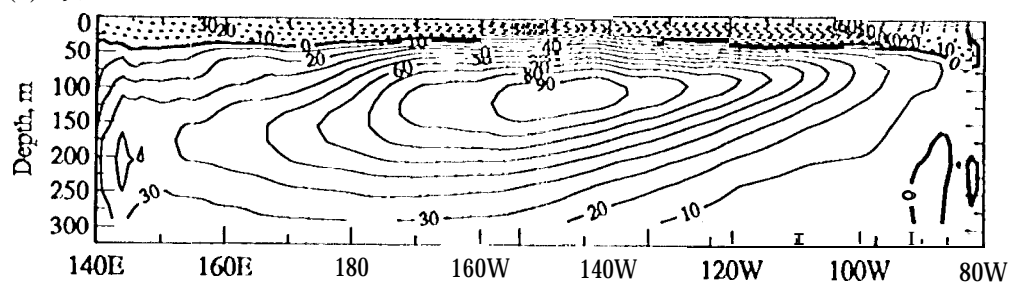
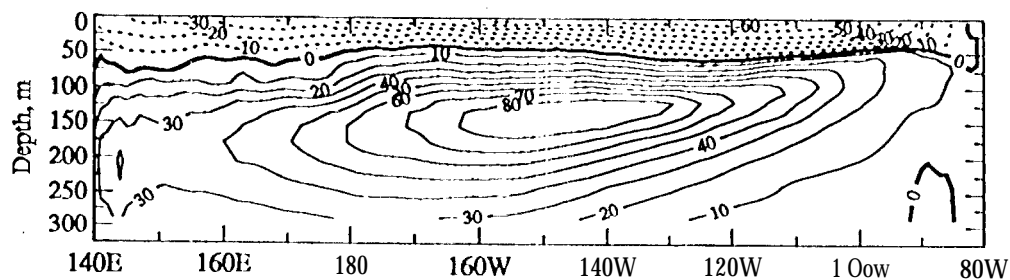


Figure 3

(a) Pj', 1988



(b) MY, 1988



(c) PP - MY, 1988

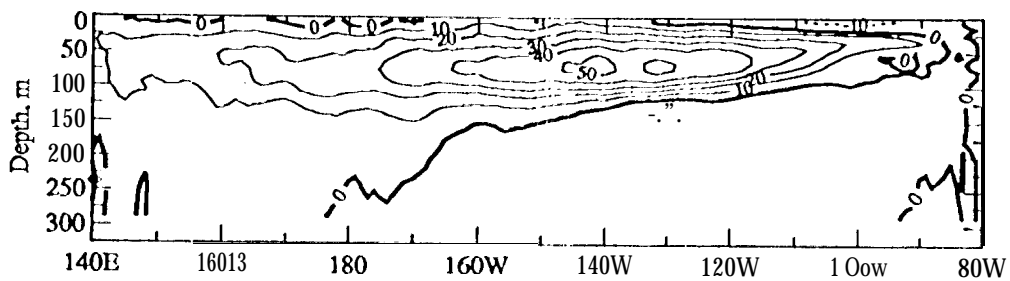


Figure 4

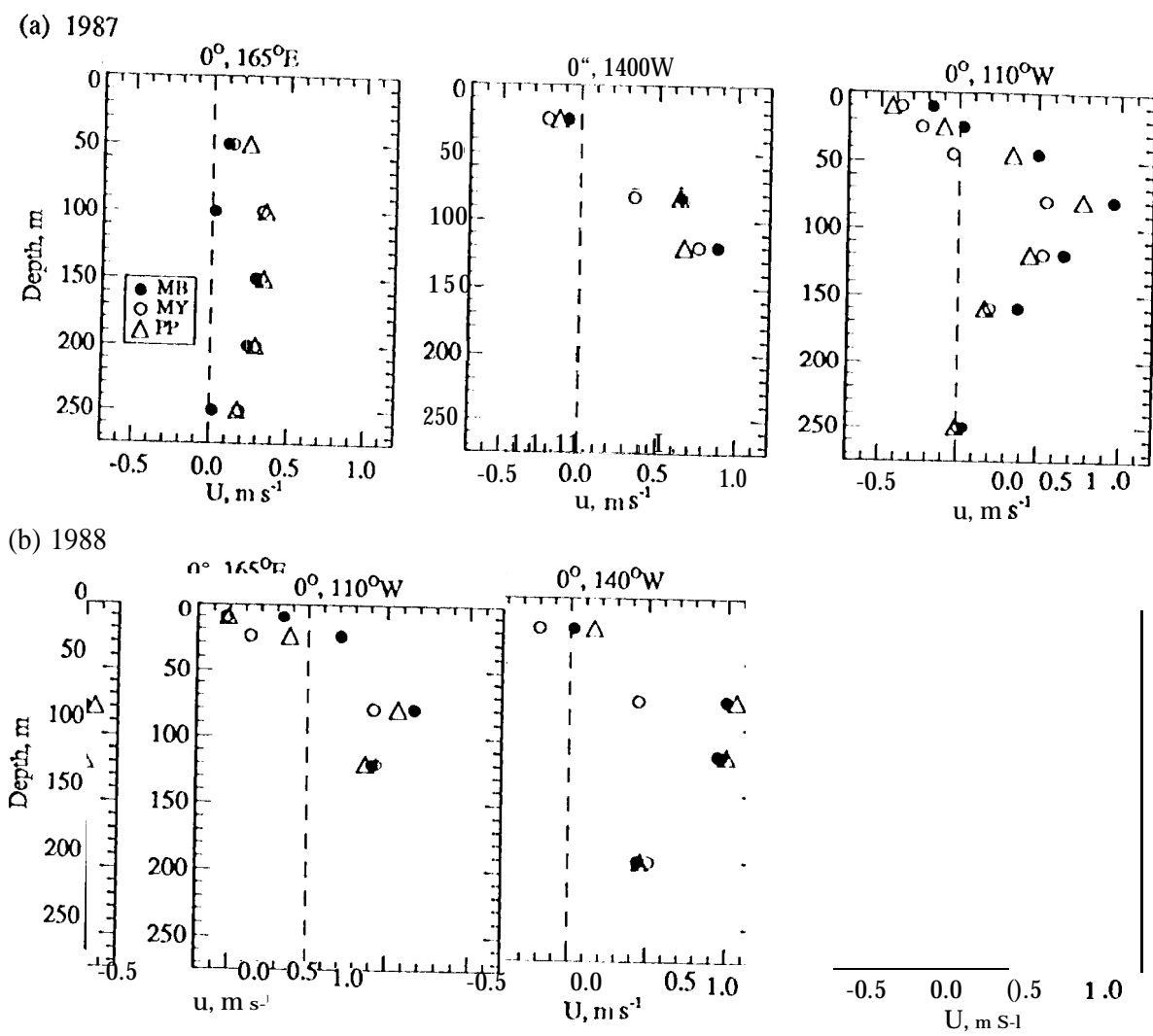


Figure 5

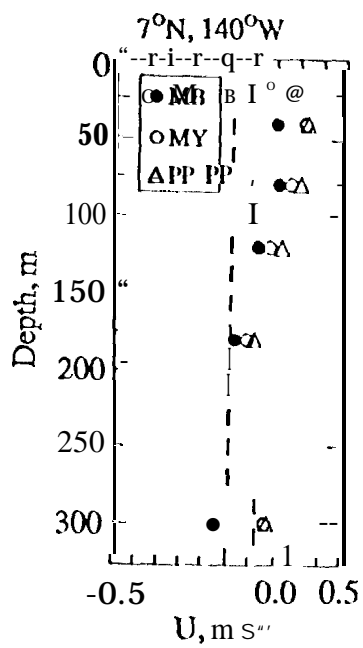


Figure 6

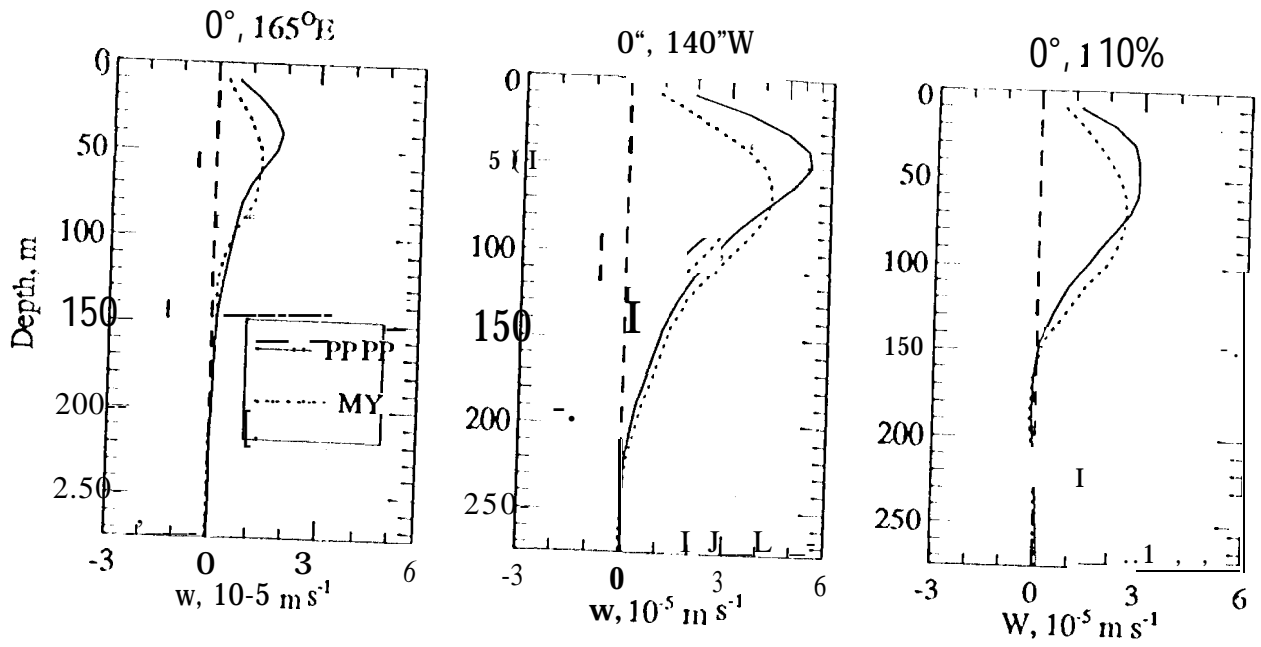


Figure 7